Initial condition effects on large scale structure in numerical simulations of plane mixing layers

W. A. McMullan and S. J. Garrett

Articles you may be interested in

Turbulent mixing of passive scalar near turbulent and non-turbulent interface in mixing layers
Phys. Fluids **27**, 085109 (2015); 10.1063/1.4928199

Investigation of Rayleigh–Taylor turbulence and mixing using direct numerical simulation with experimentally measured initial conditions. II. Dynamics of transitional flow and mixing statistics
Phys. Fluids **21**, 014107 (2009); 10.1063/1.3064121

Direct numerical simulation of a plane turbulent wall-jet including scalar mixing
Phys. Fluids **19**, 065102 (2007); 10.1063/1.2732460

Direct numerical simulation of turbulent channel flow under a uniform magnetic field for large-scale structures at high Reynolds number
Phys. Fluids **18**, 125106 (2006); 10.1063/1.2404943

Large-scale vortices in high-speed mixing layers
Phys. Fluids **15**, 3240 (2003); 10.1063/1.1602075
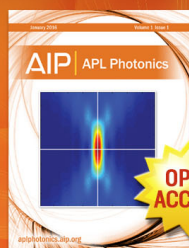
Initial condition effects on large scale structure in numerical simulations of plane mixing layers

W. A. McMullan[a] and S. J. Garrett
Department of Engineering, University of Leicester, University Road, Leicester LE1 7RH, United Kingdom

In this paper, Large Eddy Simulations are performed on the spatially developing plane turbulent mixing layer. The simulated mixing layers originate from initially laminar conditions. The focus of this research is on the effect of the nature of the imposed fluctuations on the large-scale spanwise and streamwise structures in the flow. Two simulations are performed; one with low-level three-dimensional inflow fluctuations obtained from pseudo-random numbers, the other with physically correlated fluctuations of the same magnitude obtained from an inflow generation technique. Where white-noise fluctuations provide the inflow disturbances, no spatially stationary streamwise vortex structure is observed, and the large-scale spanwise turbulent vortical structures grow continuously and linearly. These structures are observed to have a three-dimensional internal geometry with branches and dislocations. Where physically correlated provide the inflow disturbances a "streaky" streamwise structure that is spatially stationary is observed, with the large-scale turbulent vortical structures growing with the square-root of time. These large-scale structures are quasi-two-dimensional, on top of which the secondary structure rides. The simulation results are discussed in the context of the varying interpretations of mixing layer growth that have been postulated. Recommendations are made concerning the data required from experiments in order to produce accurate numerical simulation recreations of real flows. © *2016 AIP Publishing LLC.* [http://dx.doi.org/10.1063/1.4939835]

I. INTRODUCTION

For over forty years it has been known that the plane mixing layer can contain large-scale coherent structures in the high Reynolds number turbulent flow.[1] The quasi-two-dimensional vortex structures discovered by Brown and Roshko have been extensively studied experimentally, with statistics on the structure evolution,[2,3] scalar mixing,[4,5] and heat release effects,[6] all produced. These data have lead to the development of growth and entrainment,[7] and mixing models[8] that have come to gain widespread acceptance.

Doubt remains, however, as to the ubiquity of the quasi-two-dimensional, so-called "Brown-Roshko" structure. In mixing layers originating from initially turbulent upstream conditions, it has been shown that coherent structure does not appear in the flow until a significant distance downstream of the virtual origin.[9] The appearance of coherent structures in the initially turbulent flow has been linked to the aspect ratio of the mixing layer, with the far downstream end of a wind tunnel potentially enforcing some form of quasi-two-dimensionality on the mixing layer as a whole. Other research on initially laminar mixing layers has suggested that the structures can be largely irregular across the span of the flow,[10] and it has been postulated that the quasi-two-dimensional Brown-Roshko structure is formed rarely in practice; instead the mixing layer can contain essentially three-dimensional structures which undergo helical pairing interactions.[11]

Complementary to the large-scale spanwise structure in the mixing layer a secondary, streamwise orientated vortex structure was also observed in the mixing layer.[4] These structures manifest

---

[a]Electronic mail: andrew.mcmullan@le.ac.uk.

28, 015111-1

themselves as "streaks" in plan-view schlieren and shadowgraph images of the mixing layer.[12] Extensive measurement of this secondary structure shows that the locations at which the streaks form,[12–14] and the spacing of the streamwise structure,[13,15] are sensitive to the details of upstream flow conditions. The secondary structures have been observed to maintain a constant spacing over several generations of primary structure pairings[16–18] and have also been observed to increase their spacing in a stepwise manner, consistent with the evolution of the primary large-scale structure.[4,14,19] Careful measurement of the streaks has shown that the streamwise vortices can be statistically stationary,[15] and produce a well-defined wrinkling and distortion of the mixing layer across its span. The formation of streamwise vortices has been linked to small three-dimensional disturbances upstream of the splitter plate trailing edge[16] and may well be linked to residual streamwise vorticity present in the laminar boundary layer.[15] For flows undergoing helical pairings as described by Chandrsuda *et al.*,[11] it is not currently clear how the three-dimensionality of those structures can be reconciled with a statistically stationary streamwise vortex structure. An analytical study of the vortex structure in the mixing layer, through modelling of the primary rollers as Stuart vortices,[20] has highlighted two instability modes; an asymmetric mode which could potentially lead to helical pairings, and a symmetric mode resulting in the formation of a pattern of alternating-sign streamwise vortices.

The ability of numerical simulation to carefully control initial conditions (in experiments inflow conditions are denoted as initial conditions, and the two terms are used interchangeably here) and to access flow data that are difficult to attain experimentally should allow many of the outstanding issues of mixing layer evolution to be resolved. Direct Numerical Simulation (DNS) of the high-Reynolds number, spatially developing mixing layer is now within reach,[21,22] and Large Eddy Simulation (LES) has also been shown to produce accurate mixing layer data on suitably refined meshes.[23] The most challenging aspect of numerical simulation is the specification of accurate time-dependent inflow conditions. To the authors' knowledge, there exists no experimental data for mixing layers where the mean and fluctuating parts of the flow conditions at the splitter plate trailing edge are fully documented. In any numerical study, therefore, the simulated flow will be an approximation of its reference experiment, rather than being an exact numerical replication of it. Initially laminar spatial mixing layer simulation inflow conditions are typically produced from a base mean velocity profile onto which pseudo-random white noise fluctuations are superimposed at each time step.[21,23–25] In the pre-transition region, the nature of the imposed disturbances influences the nature of the laminar vortices. Three-dimensional random disturbances result in structures which undergo localised pairings, whilst highly two-dimensional random disturbances produce concentrated streamwise vortices between the primary rollers.[24] Whilst these studies were limited to the pre-transition region, more recent research has shown that simulation of initially laminar mixing layers with pseudo-random inflow disturbances leads to post-transition large-scale coherent structures which grow continuously and linearly throughout their lifetimes.[23] Flow visualisation of the high Reynolds number simulated flow shows that streamwise vorticity develops in the mixing layer and that the streamwise vorticity persists far into the turbulent region.[22,23,26,27] Evidence for the presence of statistically stationary streamwise vorticity, however, appears to be lacking in all of these spatially developing mixing layer computations.

The pseudo-random white-noise described above is neither temporally- nor spatially-correlated and is not physically representative of the background fluctuations that are present in real flows. Spatially developing simulations require an inflow generation method to produce physically correlated disturbances. Many such methods exist,[28–30] and have been applied to a wide range of flow configurations. For mixing layer simulations, inflow generation methods have been used in flows originating from initially turbulent boundary layers.[30] No published studies have used an inflow generation method to produce correlated inflow fluctuations for an initially laminar mixing layer.

This research has two aims; the first is to investigate the origin and evolution of streamwise vorticity in LES of plane mixing layers, and the second is to quantify any changes in the large-scale spanwise structure based on the nature of the streamwise vortex structures present in the flow. The initially laminar experimental conditions of Browand and Latigo[31] form the reference dataset for this study. The maximum local Reynolds number attained in the simulations, based on the visual

thickness of the mixing layer and the velocity difference across it, is $Re_\delta \approx 230\,000$. In one simulation, white-noise fluctuations provide the background disturbance environment for the flow. This type of fluctuation environment is commonly used in DNS database simulations[21,32] and in Large Eddy Simulations of the mixing layer.[23,24] A further simulation is performed where the disturbance environment is generated using a recycling and rescaling method.[30] The origin and evolution of the streamwise vorticity in both simulations will be analysed and compared to relevant experimental data where appropriate. The large-scale coherent structure evolution will be discussed in the context of the body of literature available in this field.

II. NUMERICAL METHODS

The code used in this study employs the low-Mach number approximation to simulate variable density flows in an incompressible formulation. The code is a finite-volume solver, with a staggered-cell arrangement for the primitive variables. A passive scalar (denoted $\tilde{\xi}$) transport equation is solved and is linked to the density field. Second-order central-differencing is used to compute terms in the momentum equation, whilst a second-order upwinding scheme is used for scalar convective and diffusive fluxes. The Schmidt number of the flow is set to $Sc = 0.7$. The second-order Adams-Bashforth scheme temporally advances the governing equations, with a restriction on the CFL number that it does not exceed $CFL = 0.35$ during the simulation. The pressure correction step is solved using a multi-grid method, based on a hybrid Fourier approach.

The filtering operation in Large Eddy Simulation introduces extra terms into the governing equations, which must be modelled to close the system. The subgrid stresses are modelled using the WALE model,[33] as this model has been shown to be beneficial in the simulations of mixing layers originating from initially laminar conditions.[23] The scalar transport equation is closed using the gradient diffusion model approach. The subgrid-scale Schmidt number has a constant value and is set to $Sc_t = 0.3$.

The recycling and rescaling procedure of Xiao et al.[30] is used to generate physically correlated fluctuations in case RRM. This method is similar to that of Lund et al.,[28] in that virtual domains are created upstream of the main simulation domain, in which a correlated flow field is generated and then passed into the main simulation domain. This method has been used in the literature to provide satisfactory simulated flows in a wide variety of configurations.[30,34,35]

III. PRELIMINARIES

A. Simulation setup

The initially laminar experimental conditions of Browand and Latigo[31] are shown in Table I. Although the experiments were performed at uniform density, a very minor density difference is introduced in the freestreams here in order to facilitate flow visualisations analogous to schlieren. This permits reasonably direct comparison of the simulated flow-field with those of experiments. The density ratio of the freestreams, $s = \rho_2/\rho_1 = 0.9996$, is sufficiently close to unity for the simulations presented here to be considered as ostensibly of uniform density.

In the experiment, the test section had fixed horizontal upper and lower guide-walls, which produced a small adverse pressure gradient in the flow. A representative estimate of the velocity ratio parameter, R, defined as

$$R = \frac{U_1 - U_2}{U_1 + U_2} \tag{1}$$

TABLE I. Flow parameters.

U_1 (m/s)	U_2 (m/s)	R	θ_1 (mm)	θ_2 (mm)	ρ_2/ρ_1
25.6	5.2	0.66	0.46	0.87	0.9996

is obtained using the inflow velocity values, such that $R = 0.66$. The mean streamwise velocity profile of each separating boundary layer was well-documented. Of the three components of fluctuating velocity, however, only the streamwise component was recorded and was subject to a 1% measurement error, rendering the measurement somewhat unreliable. As noted in Section I, it is therefore not possible to recreate precisely the initial conditions of this experiment.

Two distinct simulations are performed in this study; the first simulation has an inflow condition based on an imposed mean velocity profile, with the time-varying background fluctuations provided by pseudo-random white noise; the second simulation uses the inflow generation method to produce a physically correlated, time-dependent inflow condition for the mixing layer. The statistics of the flow at the trailing edge of the splitter plate are matching in each case to maintain consistency.

The main mixing layer computational domain in both cases has dimensions of $0.75 \times 0.61 \times 0.18$ (m) in the streamwise (x), vertical (y), and spanwise (z) directions, respectively. The vertical extent of the domain matches the size of the experimental facility. The domain begins at the trailing edge of the splitter plate and no solid geometry is included within it. The domain is discretised into $768 \times 256 \times 256$ cells. The mesh resolution is derived from other studies of the plane mixing layer.[23,36] The grid has a minimum spacing of $\Delta x = 0.0002$ m, and $\Delta y = 0.00004$ m in the plane of the splitter plate. The grid is stretched in the streamwise and cross-stream directions using a geometric expansion, with the spanwise nodes distributed uniformly. The high- and low-speed boundary-layers are resolved with 36 and 48 points in the cross-stream direction, respectively. The instability wavelength of the flow can be approximated as $\lambda_0 \approx 30\theta_1$,[5] and is resolved by 66 grid points. As such the initial region of the flow is extremely well-resolved. The WALE subgrid-scale model coefficient is assigned a value of $C_w = 0.56$ in this study.

The first simulation, entitled case WN (White Noise), uses only the main mixing layer domain for its calculation. The mean inflow velocity data are obtained from the experiment, as shown in Figure 1(a) for the high-speed side boundary layer. The set of fluctuation profiles shown in Figure 1(b) is imposed at the inflow plane. The nomenclature $\langle \rangle_z$ implies that a spanwise-averaging operation has been performed on the quantity. Similar profiles are also imposed in the low-speed stream. As noted above, there is insufficient experimental data to precisely recreate the initial disturbance environment; the profiles imposed here are representative of the fluctuation environment found in both experiments[31,37,38] and numerical simulations[39] of free shear flows. In case WN, these fluctuations are generated using a random number generator, and as such are both spatially- and temporally uncorrelated. Slip-wall boundary conditions are imposed on the upper and lower guide walls of the domain, and the spanwise boundaries are periodic. A standard convective outflow condition is imposed at the downstream boundary.[40] The passive scalar is assigned a value of unity in the high-speed stream, and zero in the low-speed stream. The time step of the simulation is $\Delta t = 6 \times 10^{-7}$ s. Flow statistics are gathered once the flow has attained a statistically stationary
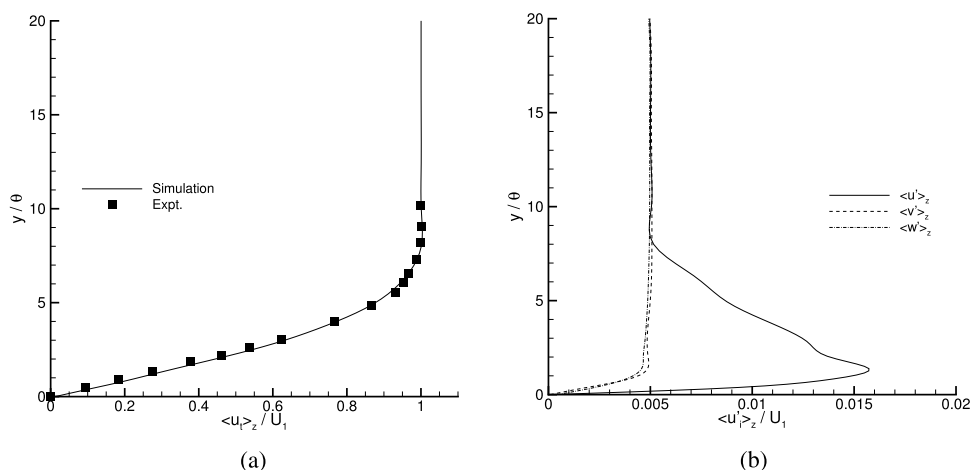

FIG. 1. Inflow profiles for the high-speed boundary layer. (a) Mean streamwise velocity. (b) Velocity fluctuations.

state over a period of twenty convective flow through times, where the convection velocity is $U_c = 0.5(U_1 + U_2)$. Spanwise-averaging of the flow statistics increases the total number of samples.

The second simulation, entitled case RRM (Recycling Rescaling Method), uses the recycling and rescaling method of Xiao *et al.*[30] to generate a time-dependent inflow condition which contains physically correlated fluctuations. Two virtual domains are created upstream of the trailing edge of the splitter plate–one for each freestream. These virtual domains extend 14δ upstream of the trailing edge, where δ is the high-speed side boundary-layer thickness. The flow at a sampling plane positioned 1δ upstream of the trailing edge is recycled onto the inlet plane at each time step, and at a given interval the entire virtual domain is rescaled to a set of target flow statistics. This correlated flow field is then used as the inflow condition to the main flow simulation. The splitter plate is modelled as a solid boundary of negligible thickness separating the two streams. The mesh resolution in the virtual domains matches that specified at the inflow plane of the main mixing layer domain described above. The flow statistics produced by this method match those imposed in case WN and are shown in Figure 1 for the high-speed stream. Similar statistics are obtained in the low-speed stream. Aside from the inflow boundary condition specification, all other simulation parameters are held constant with respect to case WN to permit valid comparisons between the two computations.

B. Validation

The validation of the present configuration closely follows that of previous work on spatially developing mixing layers.[23] For the current mesh, the simulated flow is insensitive to the choice of WALE model coefficient in the range of $0.3 \le C_w \le 0.56$. The maximum ratio of eddy to molecular viscosity reported in the simulations presented here is ~ 30 for $C_w = 0.56$, recorded at the far downstream end of the domain where the grid is at its least well refined. Near the splitter plate where the grid is highly resolved, the computed eddy viscosity is negligible in the laminar flow. Tests performed with the Smagorinsky model[41] result in a delay of the roll-up and transition of the flow when $C_s \ge 0.18$ owing to the finite eddy viscosity predicted in the initial region of the mixing layer. For a Smagorinsky model constant of $C_s = 0.1$ the bulk flow properties broadly match that of the WALE model simulations, but with a finite eddy viscosity predicted in the laminar flow region of the mixing layer. These validation tests are entirely consistent with those performed elsewhere for similar flow Reynolds numbers,[23] and are not presented here in any further detail. Validation of the spanwise domain extent shows that the aspect ratio of the flow, defined as the ratio of spanwise domain extent to local momentum thickness of the mixing layer in the domain, should not fall below a value of ten. Violating this criterion results in a flow that has its maximum spanwise wavelength confined by the spanwise domain length, and the dynamics of the coherent structures in the flow are adversely affected. A complete discussion of the confinement effect can be found elsewhere.[36] Similar estimates of aspect ratios for the spanwise domain extent required in a shear flow have been determined in other studies.[42,43]

IV. MEAN FLOW

Normalisation of the flow statistics is performed in the same manner as the reference experiment.[31] Where velocity data are non-dimensionalised by the velocity difference across the layer, $U_0 = (U_1 - U_2)$, local values of the freestream velocity are used.

The visual thickness of the mixing layer can be approximated through the superposition of many flow visualisation images and tracing the wedge swept out by the mixing layer in a mean sense.[1,5] For a uniform density mixing layer the visual thickness growth rate of the flow is expected to be a linear relationship with R, such that $\delta_{viz}/(x - x_0) = k_v R$, where x_0 is the virtual origin and k_v is a constant. In case WN, $k_v \approx 1/\pi$, a relationship that has been noted in other simulations with similar white noise disturbance environments.[23] For case RRM, the growth rate constant of $k_v \approx 0.366$ is in good agreement with the experimental data, and some 15% higher than that of case WN. It is interesting to note that the growth rate for case WN lies at the bottom of the range reported
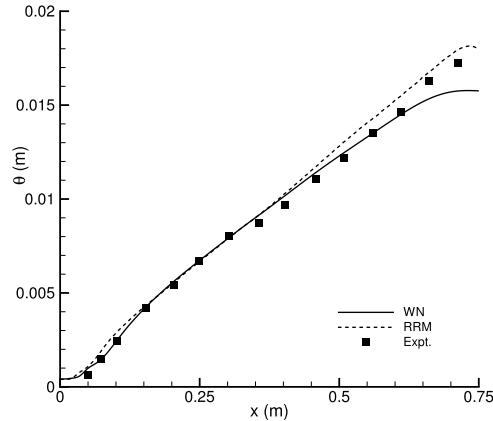
FIG. 2. Momentum thickness variation of the simulations.

in experiments, whilst that of case RRM is near the upper limit of the reported range of growth rates.[1,44]

A further measure of the growth of the mixing layer can be quantified through the momentum thickness, θ, which is defined as

$$\theta = \frac{1}{\Delta U^2} \int_{-\infty}^{\infty} (U_1 - \langle u_t \rangle_z)(\langle u_t \rangle_z - U_2) dy, \tag{2}$$

where $\langle u_t \rangle_z$ is the spanwise averaged mean streamwise velocity. The momentum thickness of each simulation is shown in Figure 2. Case WN shows reasonable agreement with the experimental data—the tailing-off of the quantity towards the downstream end of the computational domain being a common feature in simulations of shear flows with similar initial conditions.[21,23,42] Case RRM also displays good agreement with the experimental data, with the gradient of the momentum thickness curve more closely matching the experimental data in the region of 0.38 m ≤ x ≤ 0.75 m. For a uniform density mixing layer, the momentum thickness growth rate is expected to be a linear relationship, $d\theta/dx = k_m R$, in the self-similar region where k_m is a constant. The experiment reported a momentum thickness growth rate constant of $k_m \approx 0.0357$, based on an inflow velocity ratio parameter of $R = 0.66$. For case WN the constant takes a value of $k_m \approx 0.0317$, whilst for case RRM the agreement is much better, with $k_m \approx 0.036$. The discrepancies in the prediction of k_m correspond to an approximately 14% difference in the momentum thickness growth rate between the simulations.

Profiles of mean streamwise velocity and streamwise velocity fluctuations extracted from the self-similar region of the flow are presented in Figures 3(a) and 3(b). The mean streamwise velocity profiles of both simulations agree extremely well with the experiment. The streamwise velocity fluctuation data from both simulations are in good agreement with the reference data, although case RRM shows some over-prediction of the quantity in the outer regions of the mixing layer. The evolution of the peak streamwise velocity fluctuation with streamwise distance is shown in Figure 3(c). In case WN, the peak in the velocity fluctuation is predicted further downstream than in the experiment, which is typical in other simulations of shear flows.[23,39] In case RRM, however, the location of this peak is well-predicted, although the fluctuation levels in the initial region are higher than those recorded in the experiment. At $x \approx 0.32$ m both simulations attain, to within experimental error, the fluctuation level recorded in the experiment, but they attain a different self-similar state. In terms of the initial momentum thicknesses, the distance for similarity to be attained corresponds to $x/\theta_i \approx 700$, which is within the one thousand initial momentum thicknesses measure postulated by experimental research.[45]

Spectral plots of the streamwise velocity fluctuations along the plane of the splitter plate ($y = 0$) at various streamwise locations are shown in Figure 4. In case WN the energy content at $x = 0.02$ m is very low, as the white-noise disturbances rapidly decay immediately downstream of
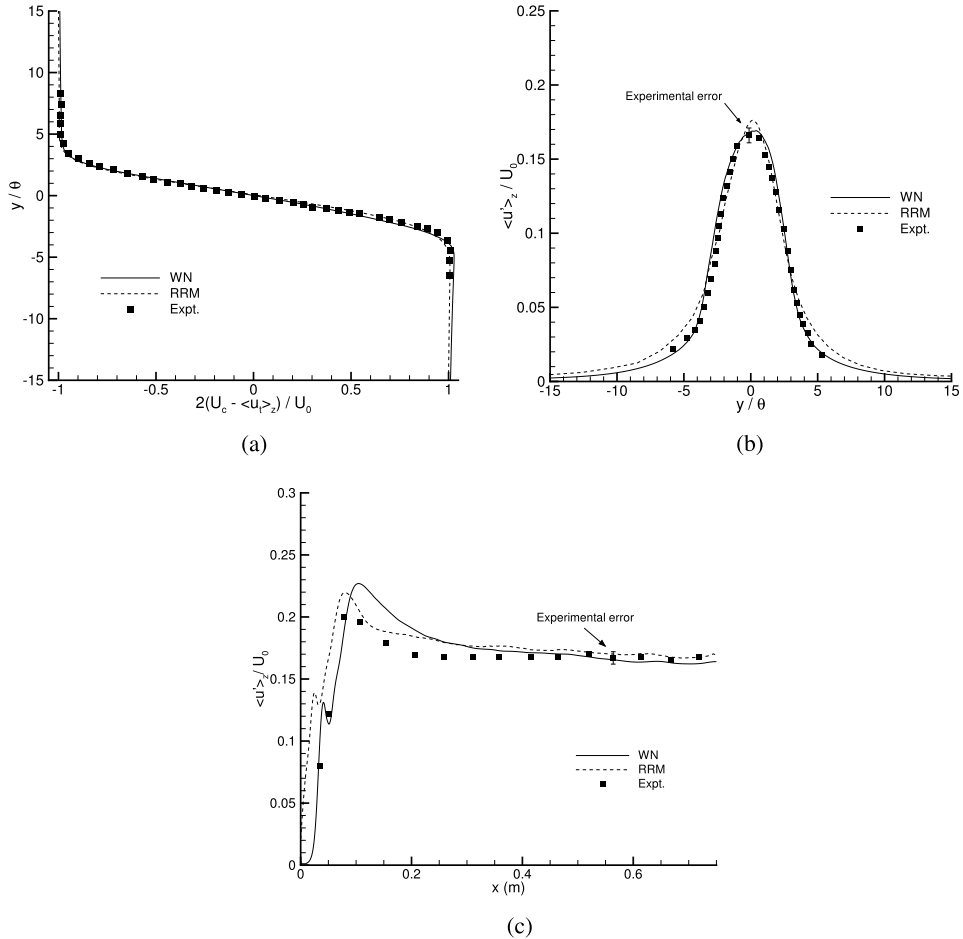
FIG. 3. (a) Mean streamwise velocity. (b) Streamwise velocity fluctuations. (c) Maximum streamwise velocity fluctuation profile.

the inflow plane. In contrast, the spectral energy content at this location in case RRM is significantly higher, as the physically correlated disturbances are able to survive.

Linear stability theory has shown that the Strouhal number of the most amplified disturbance in a two-stream mixing layer is given by
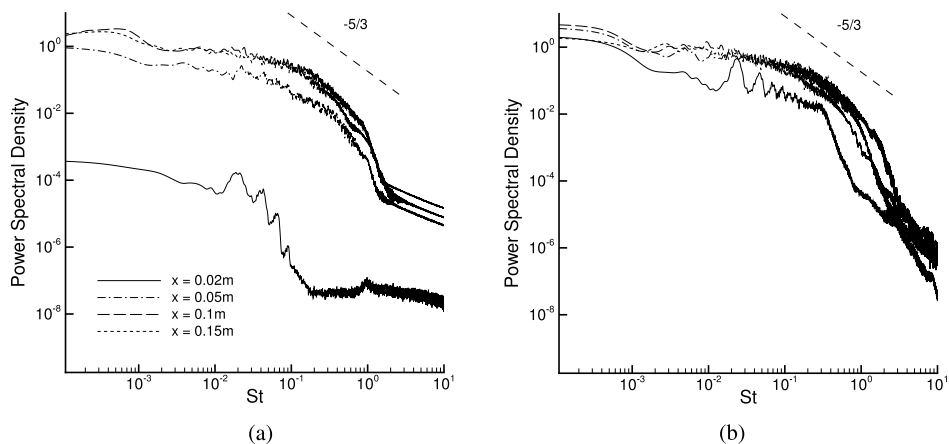

FIG. 4. Streamwise velocity fluctuation spectral plots obtained along the mixing layer centreline. (a) Case WN. (b) Case RRM.

$$\mathrm{St} \approx \frac{f \delta_\omega}{4(U_1 - U_2)} \approx \frac{0.017}{R}, \tag{3}$$

where f is the frequency, and δ_ω is the vorticity thickness.[46] For the present flow conditions, Equation (3) produces a Strouhal number of $\mathrm{St} \approx 0.0258$. At $x = 0.02$ m, peaks in the spectra are observed in both simulations. The Strouhal number of the peak instability in case RRM is $\mathrm{St} = 0.0248$, in good agreement with the theoretical value. For case WN, however, the predicted Strouhal number is $\mathrm{St} = 0.0187$, substantially lower than both the theoretical value and that obtained from case RRM. The measurement stations further downstream show that the roll-off in the spectra approach the $-5/3$ value that indicates the presence of fully developed turbulence. In the mixing layer the transition occurs as a result of an interaction between primary spanwise vortices, in the presence of a secondary streamwise structure.[47] For the present flow conditions, this typically occurs with the second interaction between primary vortices and, in a mean sense at a local Reynolds number, based on the velocity difference across the layer and its visual thickness, of $\mathrm{Re}_\delta \approx 40\,000$. This value of the local Reynolds number is in excess of the $\mathrm{Re} = 10^4$ criterion postulated for transition in mixing layers.[48]

V. STREAMWISE VORTEX STRUCTURE

Quantitative data on the streamwise vortical structure are produced from the interrogation of mean cross-plane flow fields. The flow passing through $y - z$ planes placed at intervals along the streamwise direction is recorded at a rate of 1.7 kHz. The mean streamwise vorticity is then computed directly from the ensemble-averaged cross-planes, such that $\Omega_x = \partial w_t / \partial y - \partial v_t / \partial z$, where v_t and w_t are the mean vertical and spanwise velocities, respectively. In this paper, the streamwise vorticity is partially normalised through the velocity difference across the layer, U_0, as there is no immediately obvious appropriate lengthscale for the secondary structure.[15] Where appropriate, Reynolds stresses are also computed and are normalised by the square of the velocity difference across the layer. The streamwise locations of the measurement stations expressed in terms of distance from the splitter plate trailing edge ($x = 0$), the local values of the pairing parameter, $x_i^* = Rx/30\theta_i$,[47] and the local Reynolds number, are shown in Table II. The period over which cross-plane samples are collected corresponds to the passage of 600 spanwise structures at station 2.

A. Evolution of streamwise vortex structure

Cross-plane maps of mean streamwise vorticity from case WN are shown in Figure 5. The four maps shown here are representative of those obtained from stations 2–7—the distribution of Ω_x is seemingly random with no obvious clustering into alternating bands. This lack of banding of the streamwise vorticity indicates that the streamwise structure present in case WN is not spatially stationary.

The cross-plane maps of Ω_x recorded in case RRM are shown in Figure 6. The streamwise vorticity distribution in this simulation has a markedly different character to that of case WN. At station 2 there is evidence for vertical stacking of alternating sign clusters of streamwise vorticity,

TABLE II. Measurement stations.

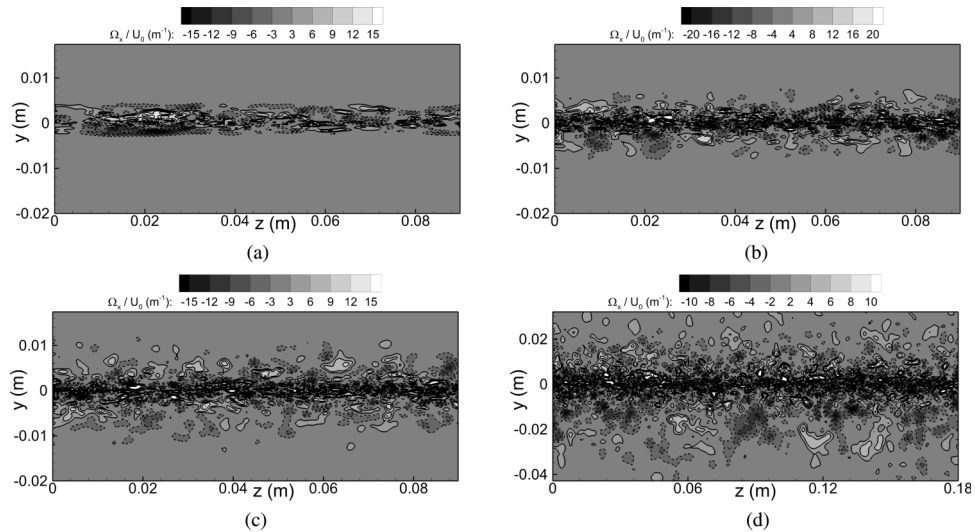| Station	x (m)	x_i^*	Re_δ (WN)	Re_δ (RRM)
1	0.02	0.96	5 900	6 600
2	0.05	2.39	14 600	16 700
3	0.10	4.78	29 400	33 500
4	0.15	7.17	44 300	50 600
5	0.30	14.34	89 000	102 000
6	0.45	21.52	136 000	154 000
7	0.60	28.70	184 000	209 000

FIG. 5. Cross-plane maps of mean streamwise vorticity in case WN. Dashed lines denote negative values. Note the changes in axes extent and contour levels. (a) $x = 0.05$ m. (b) $x = 0.1$ m. (c) $x = 0.15$ m. (d) $x = 0.45$ m.

with two like-signed clusters sandwiching a cluster of opposite sign. The vertical ordering of the stacking alternates in sign across the span. Further downstream at station 3, there is a single row of alternating sign streamwise vortices. The regular banding of the streamwise vortices demonstrates that these structures are, in a mean sense, spatially stationary. It is straightforward to trace several of the streamwise vortices from station 3 to station 4 (in particular, at $z = 0.016$, 0.022, 0.04, 0.06, and 0.075 m), and thus, the streamwise vortices can extend for a significant streamwise distance. Further downstream at station 6, the magnitude of the streamwise vorticity has reduced substantially, and it is more difficult to discern the streamwise structures. Nevertheless careful inspection of the cross planes at stations 6 and 7 shows that clustering of the low-level streamwise vorticity into alternate sign bands still persists and that the spacing of the structures has increased when compared to stations further upstream. There is some evidence of vortex merging taking place in the region of $z = 0.03$ m at station 6. The general distribution of the clusters observed in case RRM is in very good agreement with comparable experimental data.[15]
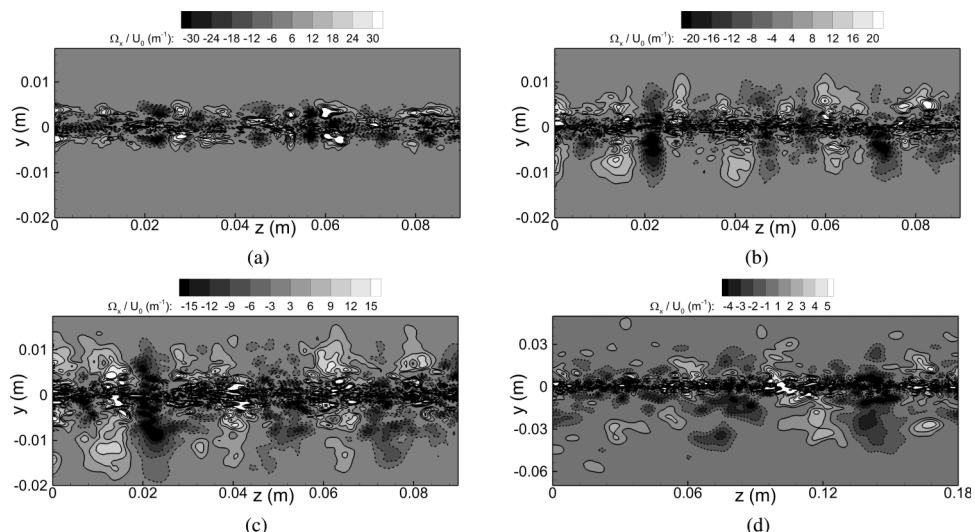

FIG. 6. Cross-plane maps of mean streamwise vorticity in case RRM. Dashed lines denote negative values. Note the changes in axes extent and contour levels. (a) $x = 0.05$ m. (b) $x = 0.1$ m. (c) $x = 0.15$ m. (d) $x = 0.45$ m.
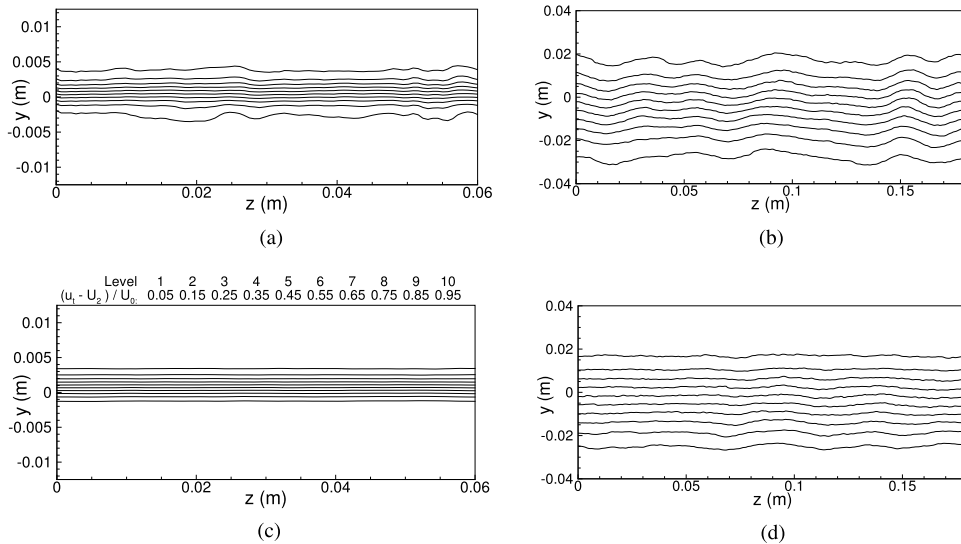
FIG. 7. Cross-plane contour maps of mean streamwise velocity. Note the changes in axes lengths. (a) Case RRM, $x = 0.05$ m. (b) Case RRM, $x = 0.3$ m. (c) Case WN, $x = 0.05$ m. (d) Case WN, $x = 0.3$ m.

Cross-plane mean streamwise velocity maps at measurement stations 2 and 5 are shown in Figure 7 for both simulations. The presence of a spatially stationary streamwise vortex structure in case RRM has a significant impact on the cross-plane mean velocity field, as the maps from this simulation show significant spanwise variations. In Figure 7(a) the velocity field shows clear evidence of wrinkling. This wrinkling of the mixing layer is caused by the transfer of streamwise momentum in the cross-stream direction by the streamwise vortices.[15] The wrinkling persists into the turbulent region of the flow, as shown in Figure 7(b) and also continues through to the final measurement station. In contrast, the maps from case WN (Figures 7(c) and 7(d)) are largely statistically two-dimensional.

The evolution of the wrinkling in the mixing layer can be assessed through plotting the locus of the mixing layer centreline across the span. The centreline of the mixing layer, y_0, is defined as the lateral vertical position where the local flow velocity is equal to the convection velocity of the flow, U_c. The locus of the mixing layer centreline along the span at each station is shown in Figure 8. In case WN (Figure 8(a)), the distribution is fairly flat near the inflow plane, with some non-uniformity appearing further downstream. There is no regular wavelength to the variations in the each profiles. The centreline profiles in case RRM are shown in Figure 8(b). At the most upstream station there are small variations in the centreline across the mixing layer. Further downstream there is a clear pattern of peaks and troughs on each locus. In experiments, peaks in the centreline distribution
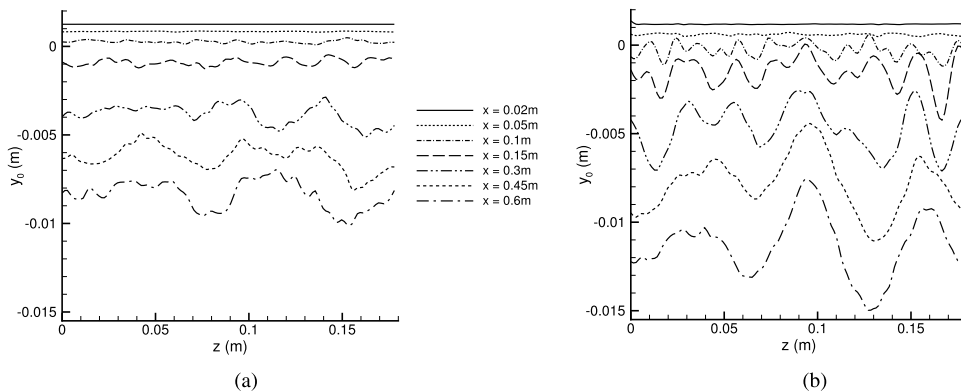

FIG. 8. Centreline locus plots at each measurement station in the simulations. (a) Case WN. (b) Case RRM.
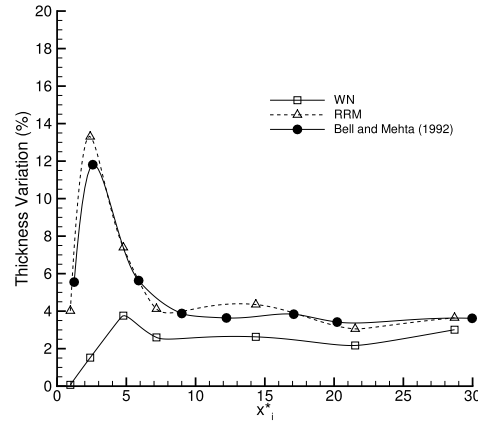
FIG. 9. Standard deviation of mixing layer thickness in the simulations. Experimental data from Bell and Mehta[15] shown for comparison.

indicated the presence of a pair of streamwise vortices with a common upflow, whilst a trough indicated a pair of streamwise vortices with a common downflow.[15] This pattern is present in case RRM; the peaks and troughs of each locus coinciding with interface between pairs of opposite-hand streamwise vorticity clusters shown in Figure 6. As the flow evolves downstream, the wavelength of the locus profile increases with the spacing of the streamwise vortices.

Quantitative information on the wrinkling of the mixing layer can be obtained by plotting the standard deviation of the mixing layer thickness as a function of streamwise distance. This quantity is plotted in Figure 9 for both simulations as a function of the pairing parameter, $x_i^* = Rx/30\theta_i$,[47] along with comparable experimental data.[15] The agreement between the data of Bell and Mehta and that of case RRM is striking. Just downstream of the splitter plate there is a low variation in the mixing layer thickness, which rapidly increases to a peak at $x_i^* \approx 2.3$. Beyond this the variation decreases until it reaches an almost constant level of 3%–4% at $x_i^* > 8$. This distribution implies that the streamwise vortices are rapidly amplified immediately following the roll up of the mixing layer into K-H vortices which occurs, on average, at $x_i^* \approx 2$. Beyond the transition, which in case RRM occurs at an average location of $x_i^* \approx 7.8$, the variation attains a near constant value, implying that the flow has become what could nominally be described as statistically two-dimensional. The stationary streamwise vortices, however, still persist far downstream in the computational domain, well into the $x > 1000\theta_i$ region that is normally considered to be the fully self-similar flow.[45] The mixing layer thickness variation of case WN is substantially different to that of case RRM–the peak of the variation occurs much further downstream, and the magnitude of the variation is significantly lower than case RRM at all streamwise stations.

The lack of obvious banding in the mean streamwise vorticity maps of case WN renders it impossible to compute a mean streamwise vortex spacing for this simulation. For case RRM, however, the mean streamwise structure spacing can be estimated by counting the bands of alternate sign Ω_x at each measurement station and calculating an average. The spacing obtained from this method is shown in Figure 10 for case RRM, along with comparable experimental data. The data of Plesniak et al.[13] and Bell and Mehta[15] were recorded in the same experimental facility, with the streams switched between tunnel legs in order to assess the effect of small changes in initial conditions on the streamwise vortex structure. The evolution of the streamwise structure spacing in case RRM follows a similar trend to that of the experimental data. The average cluster spacing at the first measurement station is 1.4 cm, which is roughly equivalent to the initial wavelength associated with the primary K-H vortices–a measurement consistent with other experimental studies.[4,15,17–19] Towards measurement station 3 the spacing decreases and subsequently increases as the flow evolves downstream. The increasing structure spacing downstream of measurement station 3 implies that some form of streamwise vortex merging or cancellation is taking place to reduce the number density. The evolution of streamwise structure spacing with streamwise distance observed in case RRM is qualitatively similar to that observed in the experiments.
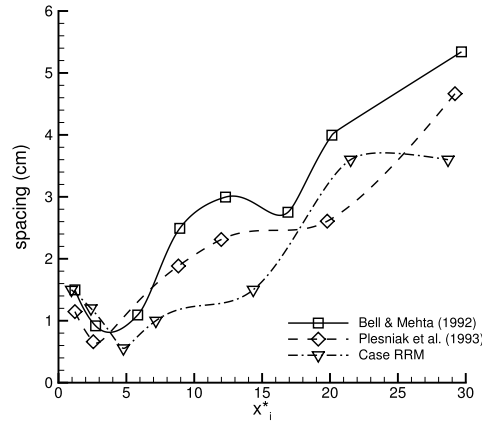
FIG. 10. Streamwise vortex structure spacing in case RRM, plotted with comparable experimental data of Plesniak *et al.*,[13] and Bell and Mehta.[15]

B. Origin of streamwise vorticity

Cross-plane contour maps of the normal Reynolds stresses ($\overline{u'^2}$, $\overline{v'^2}$, $\overline{w'^2}$) and the mean streamwise vorticity Ω_x are interrogated at measurement station 1. The contour maps obtained from case WN at this station are shown in Figure 11. Each of the normal Reynolds stresses has an extremely low magnitude at this station, with the spanwise normal stress being practically negligible. The mean streamwise vorticity map shows no particular evidence of organised structure, and the magnitude of what vorticity exists is negligible. The imposed white noise fluctuations do not spontaneously generate low-level physically correlated disturbances, leading to an initial flow region that is largely devoid of physical structure. At the next measurement station, shown in Figure 5(a), the magnitude of the mean streamwise vorticity has jumped by an order of magnitude. Between stations 1 and 2, therefore, some process must have taken place in order to generate streamwise vorticity in the mixing layer.

Instantaneous snapshots of streamwise vorticity at four distinct times in case WN, recorded at measurement station 2, are shown in Figure 12. These snapshots show the behaviour of the streamwise vorticity in what can be considered as the braid region between primary rollers. The streamwise vorticity occurs at apparently random spanwise locations with the passage of each vortex, leading to
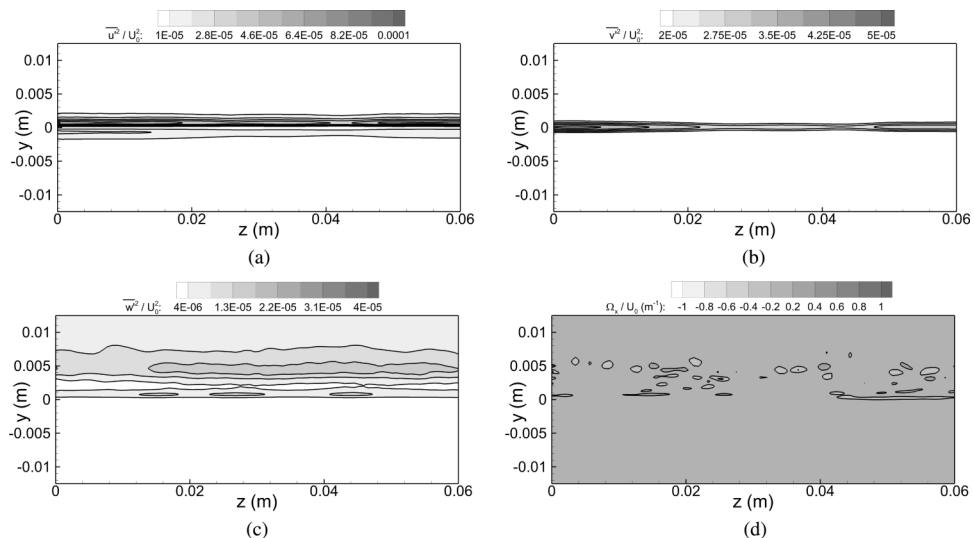

FIG. 11. Cross-plane maps at $x = 0.02$ m in case WN. Dashed lines denote negative values. One third of the spanwise extent shown for clarity. (a) $\overline{u'^2}/U_0^2$. (b) $\overline{v'^2}/U_0^2$. (c) $\overline{w'^2}/U_0^2$. (d) Ω_x.
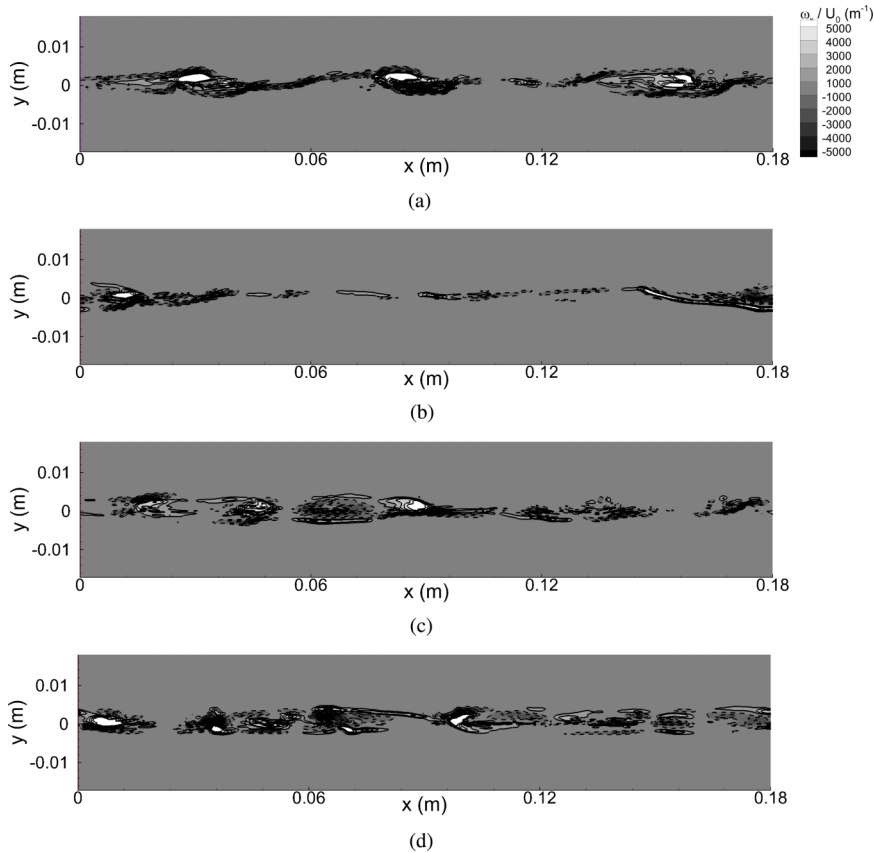
FIG. 12. Instantaneous cross-plane contours of streamwise vorticity at four random times in case WN, recorded at $x = 0.05$ m.

the lack of any organised structure in the mean contour map shown in Figure 5. As will be described in Section VI B 1, the streamwise vorticity is generated through localised pairings between primary oblique rollers.

The normal stress maps and mean streamwise vorticity recorded at station 1 in case RRM are shown in Figures 13(a)–13(d). The magnitude of the normal stresses in case RRM is some two orders of magnitude larger than that observed in case WN. There are clear peaks in each of the three normal Reynolds stress maps, and these coincide with the clustering of the mean streamwise vorticity in Figure 13(d). The clusters of Ω_x are irregularly spaced across the span of the mixing layer–in the vertical direction the streamwise vorticity contours alternate in sign across the centre-line of the mixing layer. There is some correlation between the spanwise locations of these clusters at station 1 and the clusters of streamwise vorticity found at station 2. At station 2, the flow has rolled up into K-H vortices, and the upstream residual streamwise vorticity has been amplified and is evolving into a row of stationary streamwise vortices. This pattern of streamwise vorticity development is entirely consistent with the streamwise vortex structure observed at comparable values of the pairing parameter ($x_i^* = 1.25, 2.67$) in the experiments of Bell and Mehta.[15]

The presence of low-level Ω_x at measurement station 1 indicates that some residual stream-wise vorticity must be present in flow in the region of separation from the splitter plate. As case RRM generates physically correlated fluctuations in the upstream flow, the generation technique may be responsible for generating this residual streamwise vorticity. This connection is explored in Figure 14 where the variation of the high-speed side boundary layer skin friction coefficient just upstream of the trailing edge of the splitter plate is plotted, along with the mixing layer centreline variation at station 1. Peaks in the skin friction correspond to the presence streamwise vortices in the laminar boundary layer with a common flow towards the solid surface, and troughs correspond to
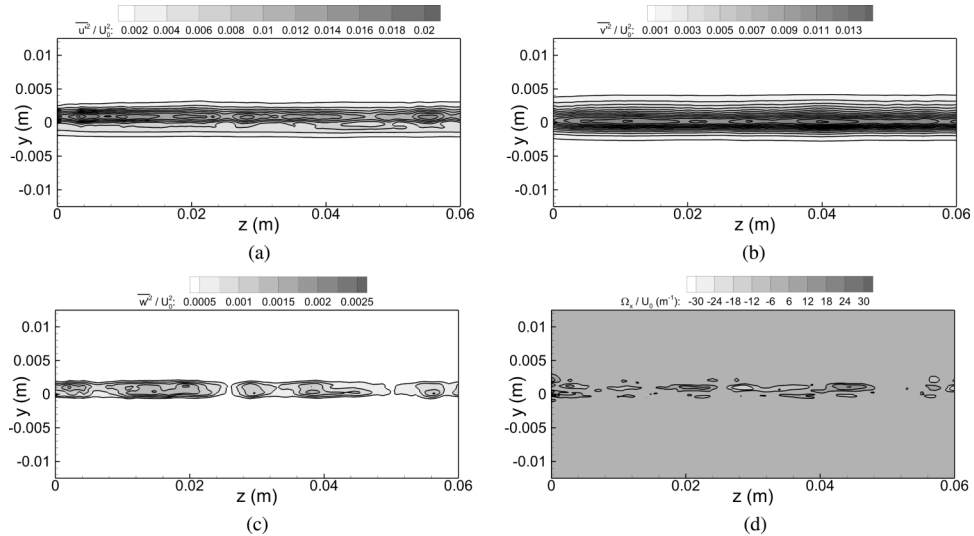
FIG. 13. Cross-plane maps at $x = 0.02$ m in case RRM. Dashed lines denote negative values. One third of the spanwise extent shown for clarity. (a) $\overline{u'^2}/U_0^2$. (b) $\overline{v'^2}/U_0^2$. (c) $\overline{w'^2}/U_0^2$. (d) Ω_x.

streamwise vortices in the laminar boundary layer with a common flow away from the surface. As described above, a peak in the mixing layer centreline distribution corresponds to a pair of stream-wise vortices with a common upflow, and a trough indicates a pair of streamwise vortices with a common downflow. There is a very clear anti-correlation in these two profiles—the peaks in the skin friction distribution align with troughs in the centreline variation, and vice versa. These plots demonstrate that weak streamwise vortices are embedded within the high-speed laminar boundary layer in case RRM, which then enter the mixing layer as the boundary layer separates from the splitter plate. This residual streamwise vorticity is then amplified by the braid instability following the roll-up of the mixing layer, producing a row of organised streamwise vorticity across the span.

VI. LARGE SCALE SPANWISE STRUCTURE

A. Flow visualisation

A sequence of up to 960 frames of flow visualisation images, sampled at a rate of 1.7 kHz, is recorded from each calculation. The vanishingly small density difference between the freestreams allows the flow to be visualised through a density gradient analogue to schlieren. Both side-view and plan-view images are obtained with the images averaged along the direction of interrogation to maintain consistency with experimental techniques.

A typical instantaneous flow visualisation from case WN is shown in Figure 15. In the side view (lower image), the initial roll-up of the flow produces pre-transition vortices. In the plan view (upper image), however, these vortices have an irregular arrangement across the span. In
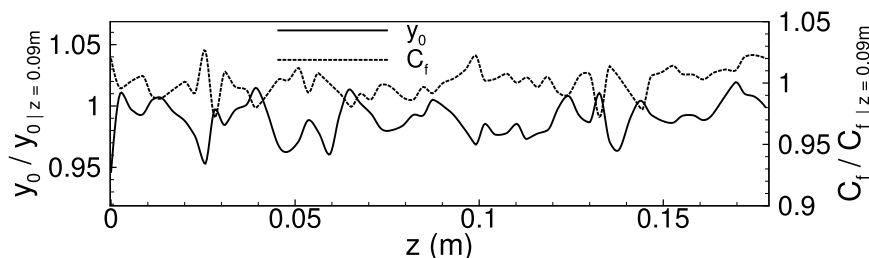

FIG. 14. Skin friction variation 0.002 m upstream of the trailing edge of the splitter plate in case RRM. Also shown is the mixing layer centreline variation, as presented in Figure 8(b).
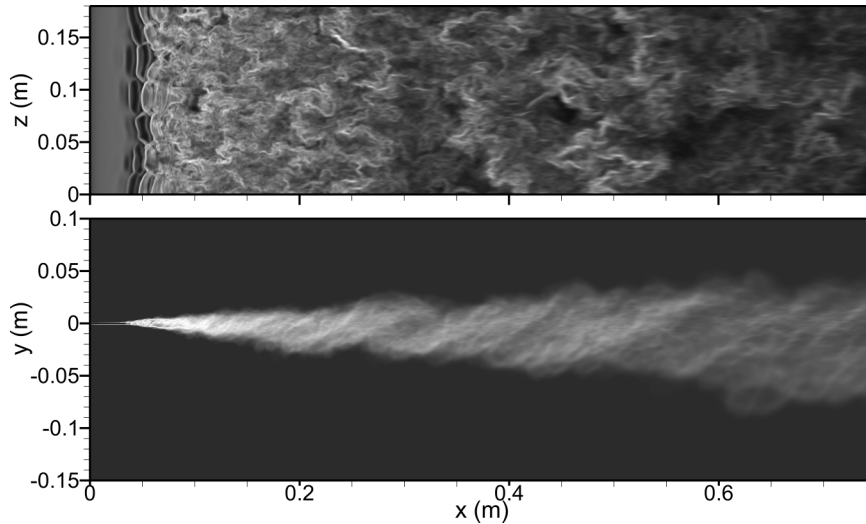
FIG. 15. Instantaneous numerical schlieren in case WN. Upper image, plan view. Lower image, side view.

this particular image, there is a clear evidence of localised pairings in the streamwise region of 0.04 m $\leq x \leq 0.07$ m across the entire span. This localised pairing can be seen in the light colours in the plan view taking a corrugated appearance in this region of the flow. This type of localised pairing has been observed in many other simulations of the plane mixing later with a pseudo-random white noise fluctuation environment,[22,24,26] and is sometimes referred to as giving the vortex structure a chain-link fence appearance. Once the streamwise structure has formed, a further interaction between the primary vortices precipitates the transition to turbulence in the mixing layer. Downstream of the transition to turbulence large-scale vortical structures are visible in the side view. The cores of the structures are visible as bumps in the side view, with thick interconnecting braid regions separating the cores. In the plan view, these large-scale spanwise structures have a complex underlying three-dimensional configuration, with a streamwise structure looping back and forth along the primary coherent structures in an irregular pattern. The overall structure observed in this image is very similar to that recorded in other simulations where white-noise disturbances formed the background fluctuations for the inflow condition.[22,23]

An instantaneous visualisation of case RRM is shown in Figure 16. This image reveals a remarkably different pattern of large-scale organisation in the mixing layer. In the initial region of the flow,
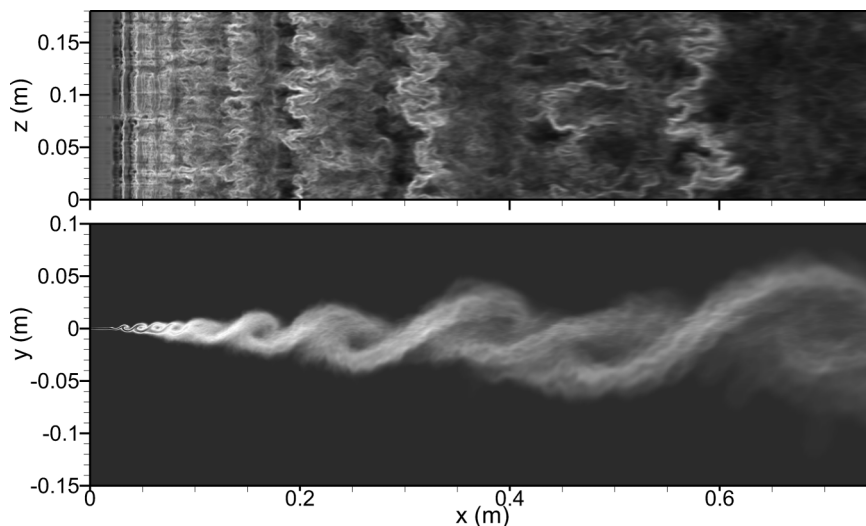

FIG. 16. Instantaneous numerical schlieren in case RRM. Upper image, plan view. Lower image, side view.

the side-view shows that the mixing layer rolls up into primary K-H vortices, with the plan view revealing that these vortices extend across the entire span, their orientation parallel to this axis. The plan view also shows the presence in the initial region of a "streaky" streamwise structure riding along with the primary spanwise rollers. These streaks are indicative of the streamwise vortices, and the visualisation demonstrates that these streaks, in this image at least, have a fairly regular spanwise appearance over a considerable streamwise distance. A pairing interaction between primary vortices triggers the transition to turbulence (at $x \approx 0.13$ m in this image), and vortical structures are clearly visible in the post-transition flow. In the side view, these turbulent vortical structures are very well-defined; each structure has a clearly identifiable core region, and thin interconnecting braid regions separate the cores. In the plan view, the secondary structure persists into the post-transition region, with its spanwise scale increasing with downstream distance. The similarity between this image and the flow visualisation image of Konrad (see Figure 9 of Bernal and Roshko[12]) is striking—the primary K-H vortices co-exist with a set of streaks of apparently regular spanwise spacing throughout the pre-transition region, whilst beyond the transition the well defined turbulent large-scale spanwise vortical structures are accompanied by a more irregular streak pattern.

These images provide qualitative evidence that a simulation with an inflow condition containing low-level pseudo-random fluctuations produces large-scale spanwise structures that are markedly different from those produced in a simulation with an inflow condition containing physically correlated fluctuations of the same magnitude. The spanwise-integrated nature of the side-view images, however, results in a loss of information on the internal structure of the large-scale spanwise structures. Other means of interrogation are therefore required in order to investigate the internal geometry of these structures.

B. Spanwise structure geometry

To study this internal vortical structure geometry a further sequence of cross-plane outputs is recorded. These samples are outputted at a frequency of 8.35 kHz and are used to produce pseudo-three-dimensional perspective views of the scalar and velocity fields in the mixing layer, similar to those reported in experiments.[19,49] The structures can deform and undergo interactions as they pass through a sampling plane, but useful information can be obtained from the perspective views when analysed in conjunction with side-view flow visualisations. Short sequences from the recorded cross-plane samples are shown in the perspective views below. In these images the high-speed side of the layer is on the upper side, with the flow from bottom left to top right of the image. An iso-surface of $\tilde{\xi} = 0.99$ defines the upper edge of the mixing layer, with the iso-surface coloured by streamwise velocity. Lighter colours denote a streamwise velocity that is higher than the freestream value, and darker colours denote a streamwise velocity that is lower than the freestream value. The appearance of an overshoot in the local streamwise velocity is associated with the passage of a large-scale vortical structure through the sampling plane.[10,49]

1. Pre-transition vortices

Short sections of the perspective views recorded at stations 2 and 3 in case WN are shown in Figures 17(a) and 17(b). These two stations reside in the pre-transition region of the mixing layer. At station 2 the primary rollers are not particularly aligned with the span, with branches and dislocations clearly visible. As vortex lines cannot end in a fluid, the branches and dislocations evident in the perspective view are caused by localised pairings between the rollers, confirming the interaction mechanism noted in the instantaneous plan view visualisation of Figure 15. Analysis of the entire sequence shows that the cycle-to-cycle spanwise location of these localised pairings is seemingly random, reinforcing the data of Figure 12, and resulting in a mean streamwise vorticity field that is not spatially stationary. These localised interactions have been observed in experiments,[11] temporal mixing layer simulations with random noise perturbations,[50] and spatially developing mixing layer simulations with inflow disturbances provided by low-level, three-dimensional random noise.[22,24,51] The perspective view recorded at station 3 (Figure 17(b)) shows that the primary vortex structure has become very irregular. Branches and dislocations in the primary structure are visible throughout
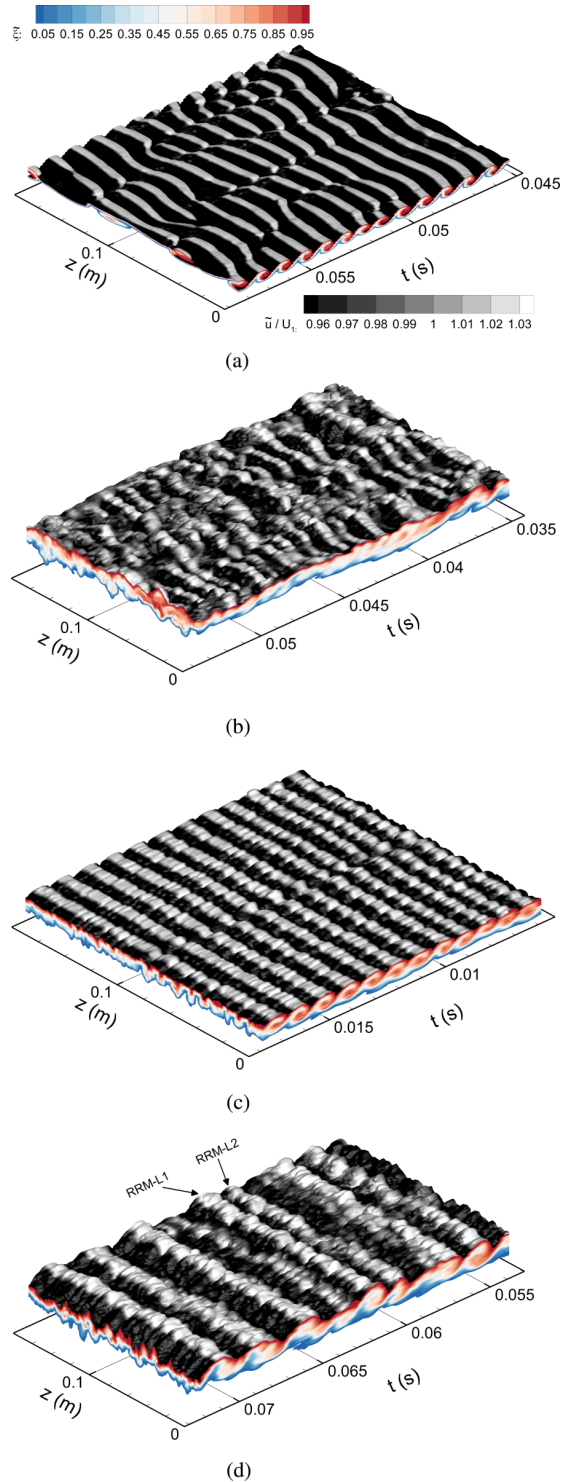
FIG. 17. Perspective views of the mixing layer in the pre-transition region. (a) Case WN, station 2. (b) Case WN, station 3. (c) Case RRM, station 2. (d) Case RRM, station 3.

the trace, indicating that localised pairings are common at this streamwise position. A similar pattern is also observed at station 4.

Sections of the perspective views recorded at measurement station 2 and 3 in case RRM are shown in Figures 17(c) and 17(d). At station 2 the primary K-H rollers in case RRM are aligned

almost perfectly parallel to the span and they occupy the entire spanwise extent of the computational domain. A secondary, streamwise-orientated structure manifests itself as undulations in the scalar iso-surface along the span primary vortices. The ridges can be traced from one spanwise roller to the next throughout the entire sample, highlighting the statistically stationary nature of the streamwise vortices in this simulation. This perspective view obtained at this station is remarkably consistent with similar visualisations obtained in a pre-transition aqueous mixing layer.[19] The perspective view at station 3 in shows that the spacing of the primary vortices in case RRM has increased, implying that an interaction between the K-H rollers has occurred between stations 2 and 3. At this measurement station the primary structures remains well-aligned with the span, and the undulations in the scalar iso-surface show a regular streamwise vortex structure superimposed on the primary vortices. The interactions between the primary spanwise vortical structures take the form of familiar K-H vortex pairings, which have been described in detail in experimental and numerical investigations of the plane mixing layer.[52,53] An example of this interaction occurs between the vortices marked RRM-L1 and RRM-L2. As these vortices pass through measurement station 3 the upstream vortex RRM-L1 has displaced vertically upwards in the flow, and its downstream neighbour RRM-L2 has displaced vertically downwards. Tripling interactions which involve three or more participating vortices have also been observed in this simulation.

2. Post-transition vortical structures

As was described in Section IV, the transition occurs in both simulations in a mean sense at a local Reynolds number, based on the velocity difference across the layer and its visual thickness, of $Re_\delta \approx 40\,000$. This is in agreement with the Reynolds number criterion outlined in previous studies.[48] The flow passing through measurement stations 5–7 will therefore consist entirely of post-transition coherent structures.

In this research, a coherent vortical structure in the turbulent flow is defined in the same manner as previous research.[23,54] When viewed in a Lagrangian frame of reference the structure has a centre of rotation, which is bounded by an upstream and downstream saddle point. The streamwise distance between the bounding saddle points defines the extent of the structure, and hence the structure spacing, l. The mean spacing of approximately 60 structures at their mid-life condition is obtained from each simulation, and the normalised structure spacing is determined. For case WN, $l/R(x - x_0) = 0.53$, and for case RRM, $l/R(x - x_0) = 0.56$. These values are in the range of normalised structure spacing values reported in experiments[1,3] and in a previous numerical simulation study.[23] In a spanwise-integrated sense, the post-transition vortical structures in cases WN and RRM have similar topographies, as can be inferred from the visualisations in Figures 15 and 16. The nature of these schlieren images necessarily averages out any underlying three-dimensionality in these structures. Perspective view images, however, can provide further useful information into the vortical structure internal geometry.

Perspective views at stations 5 and 6 obtained in case WN are shown in Figures 18(a) and 18(b). The region enclosed by the box and marked WN-T1 corresponds to the passage of the vortical structure at $x = 0.3$ m in Figure 15 through the sampling plane. This structure is typical of all those passing through this plane that do not participate in an interaction; the overshoots in the velocity field are skewed with respect to the spanwise axis, implying that the spanwise vorticity in the structure is irregularly distributed within it. The overshoots in the streamwise velocity also appear in the plane of the saddle point that separates neighbouring structures as branches between neighbouring structures. This suggests that post-transition vortical structures in case WN are able to exchange spanwise vorticity as they convect downstream. At measurement station 6 (Figure 18(b)) some dislocations are still in evidence in the perspective view, but the structures appear more quasi-two dimensional than their counterparts upstream. As the flow proceeds downstream the spanwise lengthscale of the vortical structures increases, and it is important that the spanwise domain extent of the simulation does not artificially impose a maximum spanwise wavelength on the flow. In simulations of initially laminar mixing layers with a white noise fluctuation environment, it has been observed that a local aspect ratio of $L_z/\theta > 10$ must be maintained in order to
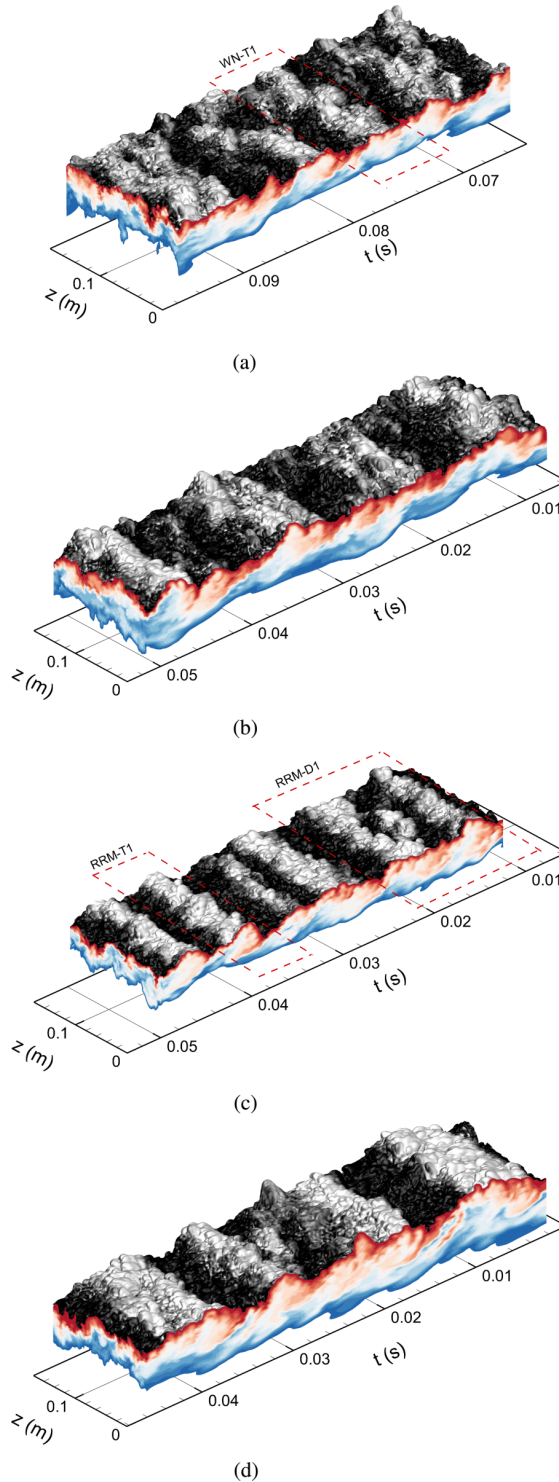
FIG. 18. Perspective views of the mixing layer in the post-transition region. (a) Case WN, station 5. (b) Case WN, station 6. (c) Case RRM, station 5. (d) Case RRM, station 6.

prevent the spanwise wavelength of the large scale structure being confined by the spanwise domain extent,[36] where L_z is the spanwise domain extent. As this criterion is never violated in the present simulation the structures at stations 6 and 7 in case WN are not artificially constrained by the spanwise extent, and evolve in the same manner as those found further upstream.

Sections of the perspective views at stations 5 and 6 from case RRM are shown in Figures 18(c) and 18(d). The boxed region in the Figure 18(c), labelled RRM-T1, marks the passage of a post-transition vortical structure through the sampling plane without undergoing an interaction. This structure is typical of all such post-transition vortical structures in case RRM. The vortical structure runs parallel to the span, and the undulations in the scalar iso-surface show the presence of a stream-wise structure. The streamwise structure is rather noticeable and runs from one structure to the next. The large-scale vortical structure in the turbulent region of case RRM can then be interpreted as large quasi-two-dimensional spanwise structures, on which a set of secondary streamwise vortices rides. In the region marked RRM-D1 there is a clear branching in the braid region between two large vortical structures. It will be shown in Section VI C that this branching is caused by a tearing interaction taking place between three neighbouring structures.

The perspective view at station 6 in case RRM is similar to that obtained at station 5–large quasi-two-dimensional structures convect through the sampling plane, with occasional branching in the vortical structures caused by tearing interactions between neighbouring structures. The perspective views obtained form the post-transition flow in case RRM are broadly similar to those obtained from a high Reynolds number aqueous mixing layer.[19]

C. Post-transition vortical structure growth and interaction

The growth of the large-scale vortical structures present in the post-transition region is ascertained through frame-by-frame analysis of the side view flow visualisations of Figures 15 and 16. Individual structures are tracked from frame to frame of the visualisation sequence, and the polar points of each structure are recorded during its lifetime. The diameter of each structure is calculated from the vertical distance between the polar points. This method has been used in previous experimental[55] and numerical[23] investigations into the turbulent mixing layer.

Growth tracks of several structures from case WN are shown in Figure 19(a). The filled symbols in this figure correspond to the growth track of structure WN-T1 shown in Figures 15 and 18(a), and the line represents the mean visual thickness of the mixing layer. Each of the structures grows continuously and linearly throughout its lifetime, with the diameter of the structures defining the self-similar growth of the mixing layer as a whole. This pattern of continuous linear growth has been reported in experiments,[55] and numerical simulations where the inflow conditions were of the same type as those of case WN.[23]

The continuous linear growth of the structures in case WN suggests that interactions between the structures has little impact on the growth of the layer. The growth tracks of two structures undergoing a post-transition merging interaction are shown in Figure 19(b). Both parent structures, WN-M1a and WN-M1b, grow continuously and linearly up until the point of interaction. The daughter structure, labelled WN-M1c, carries on with this pattern of growth. The interaction
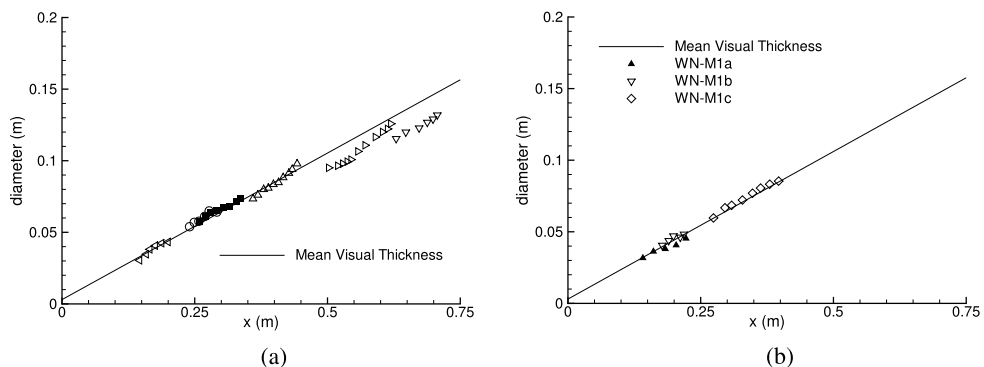

FIG. 19. Post-transition coherent structure growth in case WN. (a) Growth tracks of individual structures. Solid symbol refers to structure highlighted in Figure 18(a). (b) Case WN–merging interaction.
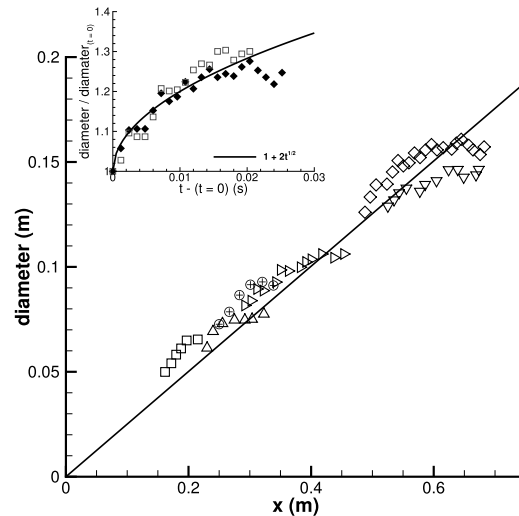
FIG. 20. Post-transition coherent structure growth in case RRM.

serves to reduce the number density of the structures and contributes nothing to the overall growth of the mixing layer. Throughout the interaction process there is no vertical displacement of the structures away from the geometric centreline of the mixing layer. Instead the centre of rotation of each parent structure remains in a fixed vertical position, the saddle point separating the two cores weakens and the two centres approach together to form a single, new centre of rotation. Interactions between the post-transition structures in case WN match those reported in McMullan *et al.*[23] Both merging- and tearing-type interactions have been observed and are described in detail elsewhere.[23]

Structure growth tracks from case RRM are shown in Figure 20. It is quite clear that the continuous growth of the post-transition structures in case RRM is not linear. Instead, the pattern of growth is better approximated through a square-root-time relationship, as shown in the inset of Figure 20. This square-root dependency is significant as it follows from past research that a vortical structure growing continuously through either irrotational roll-up,[56] or turbulent diffusion,[57] will do so as a function of the square root of time.

The square-root-time dependency on the continuous growth of the structures in case RRM implies that structure amalgamation will play a role in facilitating the overall self-similar mean growth of the mixing layer.[56] Qualitative inspection of the structures in the flow visualisation images (such as Figure 16) shows that there is some vertical displacement of the structure cores from the geometric centreline of the mixing layer. These deviations imply that the structures undergo some level of rotation around a common centre during interactions. A typical example of a pairing interaction is shown in Figure 21. Two post-transition structures, RRM-P1a and RRM-P1b, begin to undergo an interaction in Figure 21(a), with the upstream structure displacing upwards in the flow. There is a corresponding downwards displacement of the centre of rotation of the downstream structure. The saddle point separating the cores weakens and following some rotation of the cores around a common centre, the cores merge together forming a new structure, denoted RRM-P1c. Growth tracks of the structures participating in this interaction are shown in Figure 21(d). Structure RRM-P1a is at the beginning of its life and is therefore growing rapidly, whilst structure RRM-P1b reaches the end of its life and its growth rate has diminished. One formed, the daughter structure commences a pattern of square-root-time growth that matches those shown in Figure 20.

Tearing interactions also occur between three structures in case RRM. An example of this interaction is highlighted as RRM-D1 in the perspective view of Figure 18(c), where a dislocation is sandwiched between two large vortical structures. A sequence of side-view visualisation images that capture this interaction is shown in Figure 22. Structure RRM-D1b is torn apart by the
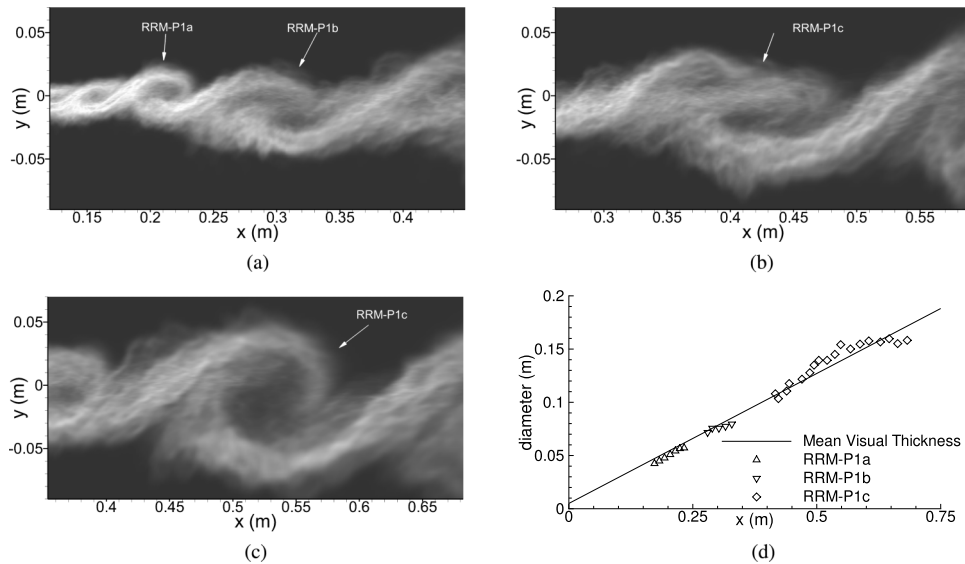
FIG. 21. Post-transition coherent structure pairing interaction in case RRM.

neighbouring structures RRM-D1a and RRM-D1c. In Figure 22(a), the structure labelled RRM-D1a is in fact two structures that are undergoing a pairing interaction—a process that has completed in Figure 22(b). The tearing of structure RRM-D1b results in its disappearance from the flow, and a braid region occupies the space left by it. The streamwise extent of structures RRM-D1a and RRM-D1c increases as a result of the interaction in order to occupy the space vacated by RRM-D1b. The growth tracks of the structures in this tearing interaction are shown in Figure 22(d). The growth of the sacrificial structure, RRM-D1b, tails off as the interaction process begins. As RRM-D1b is bled into the neighbouring structures, the continuous growth periods of structures RRM-D1a and RRM-D1c are extended. In the case of RRM-D1c, the continuous growth persists for the remainder of is passage through the computational domain. The track of RRM-D1a terminates when it begins a pairing interaction with its upstream neighbour. The growth of structure RRM-D1c during this tearing interaction is approximately linear, albeit at a rate that is significantly lower than the mean visual thickness growth rate.
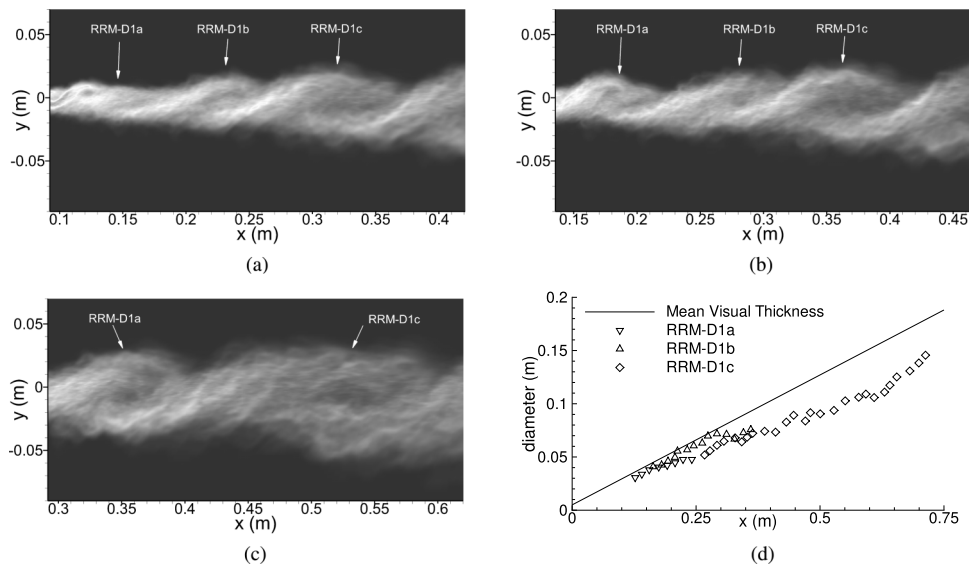

FIG. 22. Post-transition coherent structure tearing interaction in case RRM.

VII. DISCUSSION

For statistically identical initial (or inflow) conditions, the modest discrepancies in the reported mean-flow statistics of cases WN and RRM belie dramatic changes in the flow evolution and internal geometry between the simulations.

From a simulation perspective, case WN affirms the relationship between the imposed low-level, three-dimensional white-noise fluctuations and the oblique laminar vortex rollers observed in other temporally- and spatially-developing mixing layers.[22,24,51] The localised pairings between the primary oblique rollers do not occur at fixed spanwise locations, resulting in a mean streamwise vorticity field that is not statistically spatially stationary. Following the transition to turbulence in the mixing layer, the perspective views show that the large scale spanwise vortical structures have a complex internal geometry, with branches appearing in the braid regions between neighbouring structures. From these perspective views it can be inferred that the internal geometry of the coherent structures in case WN can provide a mechanism by spanwise vorticity is exchanged between structures, facilitating the linear growth observed in the side-view visualisations. Case WN also displays an absence of "classical pairing-type" interactions between primary spanwise structures in the turbulent flow, as vertical displacement of the structures in the mixing layer is not observed.

In contrast, the imposition of physically correlated, low-level three-dimensional fluctuations in case RRM leads to a pre-transition flow that consists of spanwise K-H vortices on which a secondary streamwise structure is superimposed. The roll-up of the flow into discrete vortices amplifies the residual streamwise vorticity present in the separating high-speed boundary layer into a single row of alternating-sign streamwise vortices. These streamwise vortices are then observed to evolve in a manner consistent with those recorded in experiments.[13,15] Throughout the entire streamwise extent simulated in case RRM, both the laminar K-H rollers and the turbulent large-scale spanwise vortex structures are aligned parallel to the spanwise axis and are effectively quasi-two-dimensional. From theoretical analyses it has been demonstrated that a two-dimensional vortex should grow as the square root of time,[56,57] which is the observed pattern of large-scale spanwise structure growth in the structures in case RRM.

Given that the coherent structures in the mixing layer occupy the entire visual thickness of the flow, it is obvious that their dynamics will play a dominant role in the self-similar growth rate of the mixing layer. The contrasting structure dynamics in the simulations reported here results in significantly different mean growth rates between the calculations. In case WN where the post-transition structures grow continuously and linearly and no classical pairings are observed, the mean visual thickness growth rate is defined by the rate at which linear growth of the structures occurs. Modelling the linearly growing structures as circles that have a linear rate of growth of diameter, it follows that the rate of growth of the structure will be $1/\pi \approx 0.32$.[23] In case RRM, the mean self-similar growth is obtained from continuous square-root-time growth of the quasi-two-dimensional turbulent spanwise structures, along with interactions that serve to re-concentrate structure cores. The randomness of the locations of the interactions serves to disguise the square-root-time growth of the individual structures into an overall linear mean self-similar growth of the mixing layer. The pairing interactions that take place between the large-scale spanwise structures involve some vertical displacement of the structures in the mixing layer, and bodily merging of the parent vortical structures to form a larger structure. In tearing interactions, vorticity is bled from the sacrificial structure into its neighbours. Temporal mixing layer simulations have also noted that a turbulent mixing layer undergoing classical pairing-type interactions has an approximately 20% increased growth rate when compared to a turbulent mixing layer that has an absence of classical-type pairings.[58] In that study, the layer with structures participating in pairings had thin interconnecting braid regions devoid of spanwise vorticity, whilst the flow with an absence of such pairings had thick interconnecting braids containing significant amounts of spanwise vorticity. From the perspective views of the simulations presented here, it can be inferred that spanwise vorticity exists in the thickened braids of case WN (where no classical pairings take place) and that little spanwise vorticity exists in the braids of case RRM, where the structures do undergo classical pairing-type interactions.

The presence of organised large-scale spanwise vortical structures in the plane turbulent mixing layer has long been a topic of controversy in academic research. The discovery of these structures by Brown and Roshko[1] sparked widespread interest in both understanding their dynamics, and whether the structures were ubiquitous over the range of Reynolds numbers. As described in Section I the quasi-two-dimensional Brown-Roshko structure was subsequently observed in a wide variety of flow conditions. Other experiments, however, observed structures that were more three dimensional in their spanwise structure,[10] and some studies suggested that the Brown-Roshko structure was unusual in practice, with three-dimensional structures undergoing helical interactions being more commonplace.[11] It is clear from the Caltech visualisations of the uniform density mixing layer[4,12] that quasi-two-dimensional large-scale structures are readily apparent in side view images of the post-transition flow when a streaky streamwise structure is visible in the plan view. There is a striking resemblance between the Caltech visualisations and the outputs from case RRM, and the statistical properties of both the streamwise vortices and large-scale spanwise structures are in good agreement with data from those experiments.[12] We propose that the structures present in case RRM are the same quasi-two-dimensional vortical structures observed in the Caltech experiments. It has been postulated that the streamwise streaky structure has, at best, a very weak influence in the overall two-dimensional mechanics of the large spanwise structures.[59] The evidence from case RRM presented here supports this interpretation of the post-transition flow dynamics, as the quasi-two-dimensional post-transition structures in case RRM undergo pairing and tearing interactions that are similar in form to their pre-transition counterparts.[52]

An alternative interpretation of the evolution of the turbulent mixing layer, however, has also been presented.[55] In these experiments the post-transition vortical structures in the uniform density mixing layer grew continuously and linearly throughout their lifetimes, with structure interactions serving only to reduce the number density of the structures and to facilitate the continuous linear growth. This view of the mixing layer is incompatible with a two-dimensional interpretation of the flow, as there is no obvious mechanism by which the structures can grow continuously if the spanwise vorticity is condensed into (quasi-)two-dimensional clumps. The continuous linear growth of the structures in both case WN and other similar simulations[23] supports the measurements obtained from these experiments and suggests that the post-transition coherent structures in those uniform density experiments had a three-dimensional internal geometry, permitting their continuous linear growth. We postulate that the three-dimensional coherent structures present in case WN are of the same form as those observed in the uniform density experiments of D'Ovidio and Coats.[55] It is interesting to note that the uniform density visual thickness growth rates reported by Brown and Roshko[1] are approximately 13% higher than those observed by D'Ovidio and Coats[55] for the uniform density flow. This difference in growth rate is similar to that reported between cases RRM and WN, where a mixing layer containing quasi-two-dimensional post-transition structures has a 15% higher growth rate than one which contains inherently three-dimensional coherent structures. We therefore postulate that the differences in reported growth rates of the uniform density mixing layer originating from initially laminar conditions may be caused by differences in the coherent structure evolution in those experiments.

In real flows, of course, the initial conditions will contain background disturbances that are physically correlated. Although case WN produces the same continuous linear growth observed in the experiments of D'Ovidio and Coats,[55] there is a clear disconnect between the nature of the fluctuation environment in case WN and the physically correlated fluctuation environment of the experiment. Further investigation is required in order to ascertain the connection between physically realistic simulation inflow conditions and the observed continuous linear growth of the turbulent mixing layer in experiments.

Concerning the streamwise vortices, experimental research has demonstrated that the origin of streamwise vorticity in the mixing layer is influenced by the flow upstream of the splitter plate trailing edge. It has been shown experimentally that small changes in the flow field (through changing of screens, or flipping the freestreams in the wind tunnel for example) can produce marked changes in the positioning of the streaks in both flow visualisation images,[12] and in the statistical quantities of the streamwise vortices.[13] The persistence of the streamwise vorticity into the fully developed region prompted Bell and Mehta to suggest that the criterion for self-similarity may need to be

re-evaluated. They also suggested that "*The effect of streamwise vorticity on the near-field behaviour of the mixing layer is sufficiently strong that the streamwise vortex structure should be included in all modelling of mixing layers originating from laminar initial boundary layers.*"[15] In light of the findings in the present study, this remark made by Bell and Mehta is very prescient indeed. In order to successfully achieve this, however, far more quantitative information on the initial conditions of experiments is required in order to accurately re-create reference experimental data. As a suggested minimum, information on the mean streamwise velocity profile, and the associated velocity fluctuation profiles in each of the three velocity components are essential.

VIII. CONCLUSIONS

Large Eddy Simulation has been used to investigate the both the streamwise and spanwise structures in the plane turbulent mixing layer. The simulations show that the nature of the imposed fluctuations in the simulation inflow conditions has a substantial effect on both the origin and evolution of streamwise vorticity in the flow, and the evolution of the large-scale spanwise vortex structures in the post-transition flow. A simulation with low-level, three-dimensional pseudo-random inflow disturbances results in a mixing layer with a spatially non-stationary streamwise vortex structure, and three-dimensional post-transition coherent structures that grow continuously and linearly. A simulation with physically correlated disturbances of the same magnitude produces a mixing layer with a statistically stationary streamwise vortex structure, and quasi-two-dimensional post-transition structures that grow with the square root of time. These results indicate a hyper-sensitivity of the spatially developing mixing layer to its imposed initial conditions, and demonstrate that our understanding of this sensitivity is currently incomplete.

ACKNOWLEDGMENTS

[1] G. L. Brown and A. Roshko, "On density effects and large structure in turbulent mixing layers," J. Fluid Mech. **64**, 755–816 (1974).

[2] L. P. Bernal, "The coherent structure of turbulent mixing layers," Ph.D. thesis, California Institute of Technology, 1981.

[3] M. A. Hernan and J. Jimenez, "Computer analysis of a high-speed film of the plane turbulent mixing layer," J. Fluid Mech. **119**, 323–345 (1982).

[4] J. H. Konrad, "An experimental investigation of mixing in two-dimensional turbulent shear flows with applications to diffusion-limited chemical reactions," Ph.D. thesis, California Institute of Technology, 1976.

[5] P. S. Karasso and M. G. Mungal, "Scalar mixing and reaction in plane liquid shear layers," J. Fluid Mech. **323**, 23–63 (1996).

[6] J. C. Hermanson and P. E. Dimotakis, "Effects of heat release in a turbulent, reacting shear layer," J. Fluid Mech. **199**, 333–375 (1989).

[7] P. E. Dimotakis, "Two-dimensional shear layer entrainment," AIAA J. **24**, 1791–1796 (1986).

[8] J. E. Broadwell and R. E. Breidenthal, "A simple model of mixing and chemical reaction in a turbulent shear layer," J. Fluid Mech. **125**, 397–410 (1982).

[9] M. D. Slessor, C. L. Bond, and P. E. Dimotakis, "Turbulent shear-layer mixing at high Reynolds numbers: Effects of inflow conditions," J. Fluid Mech. **376**, 115–138 (1998).

[10] F. K. Browand and T. R. Troutt, "The turbulent mixing layer: Geometry of large vortices," J. Fluid Mech. **158**, 489–509 (1985).

[11] C. Chandrsuda, R. D. Mehta, A. D. Weir, and P. Bradshaw, "Effect of free stream turbulence on large structure in turbulent mixing layers," J. Fluid Mech. **85**, 693–704 (1978).

[12] L. P. Bernal and A. Roshko, "Streamwise vortex structure in plane mixing layers," J. Fluid Mech. **170**, 499–525 (1986).

[13] M. W. Plesniak, J. H. Bell, and R. D. Mehta, "Effects of small changes in initial conditions on mixing layer three-dimensionality," Exp. Fluids **14**, 286–288 (1993).

[14] J. Jimenez, "A spanwise structure in the plane shear layer," J. Fluid Mech. **132**, 319–336 (1983).

[15] J. H. Bell and R. D. Mehta, "Measurement of streamwise vortical structures in a plane mixing layer," J. Fluid Mech. **239**, 213–248 (1982).

[16] J. C. Lasheras, J. S. Cho, and T. Maxworthy, "On the origin and evolution of streamwise vortical structures in a plane, free shear layer," J. Fluid Mech. **172**, 231–258 (1986).

[17] R. Breidenthal, "Structure in turbulent mixing layers and wakes using a chemical reaction," J. Fluid Mech. **109**, 1–24 (1981).

[18] J. C. Lasheras and H. Choi, "Three-dimensional instability of a plane free shear layer: An experimental study of the formation and evolution of streamwise vortices," J. Fluid Mech. **189**, 53–86 (1988).

[19] J. Jimenez, M. Cogollos, and L. P. Bernal, "A perspective view of the plane mixing layer," J. Fluid Mech. **152**, 125–143 (1985).

[20] R. T. Pierrehumbert and S. E. Widnall, "The two- and three-dimensional instabilities of a spatially periodic shear layer," J. Fluid Mech. **114**, 59–82 (1982).

[21] A. Attili and F. Bisetti, "Statistics and scaling of turbulence in a spatially developing mixing layer at Re$_\lambda$ = 250," Phys. Fluids **24**, 035109 (2012).

[22] Y. Wang, M. Tanahashi, and T. Miyauchi, "Coherent fine scale eddies in turbulence transition of spatially-developing mixing layer," Int. J. Heat Fluid Flow **28**, 1280–1290 (2007).

[23] W. A. McMullan, S. Gao, and C. M. Coats, "Organised large structure in the post-transition mixing layer. Part 2. Large eddy simulation," J. Fluid Mech. **762**, 302–343 (2015).

[24] M. Lesieur, P. Comte, E. Lamballais, O. Metais, and G. Silvestrini, "Large-eddy simulations of shear flows," J. Eng. Math. **32**, 195–215 (1997).

[25] W. A. McMullan, S. Gao, and C. M. Coats, "The effect of inflow conditions on the transition to turbulence in large eddy simulations of spatially developing mixing layers," Int. J. Heat Fluid Flow **30**, 1054-1066 (2009).

[26] P. S. Bernard, "Grid-free simulation of the spatially growing turbulent mixing layer," AIAA J. **46**, 1275–1737 (2008).

[27] S. Laziet, S. Lardeau, and E. Lamballais, "Direct numerical simulation of a mixing layer downstream a thick splitter plate," Phys. Fluids **22**, 015104 (2010).

[28] T. Lund, X. Wu, and D. Squires, "Generation of turbulent inflow data for spatially developing boundary layer simulations," J. Comput. Phys. **140**, 233–258 (1998).

[29] M. Klein, A. Sadiki, and J. Janicka, "A digital filter based generation of inflow data for spatially developing direct numerical or large eddy simulation," J. Comput. Phys. **186**, 652–665 (2003).

[30] F. Xiao, M. Dianat, and J. J. McGuirk, "A recycling/rescaling method for LES inlet condition generation," in *Proceedings of the 8th International ERCOFTAC Symposium on Engineering Turbulence Modelling and Measurements, Marseille, France* (2010), pp. 510–515.

[31] F. K. Browand and B. O. Latigo, "Growth of the two-dimensional mixing layer from a turbulent and nonturbulent boundary layer," Phys. Fluids **22**, 1011–1019 (1979).

[32] A. Attili, C. Cristancho, and F. Bisetti, "Statistics of the turbulent/non-turbulent interface in a spatially-developing mixing layer," J. Turbul. **15**, 555–568 (2014).

[33] F. Nicoud and F. Ducros, "Subgrid-scale stress modelling based on the square of the velocity gradient tensor," Flow, Turbul. Combust. **62**, 183–200 (1999).

[34] P. C. Wang and J. J. McGuirk, "Large eddy simulation of high speed nozzle flows–assessment and validation of synthetic turbulence inlet conditions," AIAA Paper 2011-3555, 2011.

[35] F. Xiao, M. Dianat, and J. J. McGuirk, "LES of turbulent liquid jet primary breakup in turbulent coaxial flow," Int. J. Mulitphase Flow **60**, 103–118 (2014).

[36] W. A. McMullan, "Spanwise domain effects on the evolution of the plane turbulent mixing layer," Int. J. Comput. Fluid Dyn. **29**, 333–345 (2015).

[37] L. M. Pickett and J. B. Ghandhi, "Passive scalar mixing in a planar shear layer with laminar and turbulent inlet conditions," Phys. Fluids **14**, 985–996 (2002).

[38] A. K. M. F. Hussain and M. F. Zedan, "Effects of the initial condition on the axisymmetric free shear layer: Effect of the initial fluctuation level," Phys. Fluids **21**, 1475–1481 (1978).

[39] C. Bogey and C. Bailly, "Influence of nozzle-exit boundary-layer conditions on the flow and acoustic fields of initially laminar jets," J. Fluid Mech. **663**, 507–538 (2010).

[40] P. Voke and S. G. Potamitis, "Numerical simulation of a low-Reynolds-number turbulent wake behind a flat plate," Int. J. Numer. Methods Fluids **19**, 377–393 (1994).

[41] J. Smagorinsky, "General circulation experiments with the primitive equations I. The basic experiment," Mon. Weather Rev. **91**, 99–164 (1963).

[42] L. Biancofiore, "Crossover between two- and three-dimensional turbulence in spatial mixing layers," J. Fluid Mech. **745**, 164–179 (2014).

[43] B. Thornber, "Impact of computational domain size in simulations of homogeneous decaying turbulence and mixing layers," AIAA Paper 2015-3430, 2015.

[44] D. A. Yoder, J. R. DeBonis, and N. J. Georgiadis, "Modeling of turbulent free shear flows," Comput. Fluids **117**, 212–232 (2015).

[45] P. Bradshaw, "The effect of initial conditions on the development of a free shear layer," J. Fluid Mech. **26**, 225–236 (1966).

[46] P. A. Monkewitz and P. Huerre, "Influence of velocity ration on the spatial instability of mixing layers," Phys. Fluids **25**, 1137–1143 (1982).

[47] L. S. Huang and C. M. Ho, "Small-scale transition in a plane mixing layer," J. Fluid Mech. **210**, 475–500 (1990).

[48] P. E. Dimotakis, "The mixing transition in turbulent flows," J. Fluid Mech. **409**, 69–98 (2000).

[49] F. K. Browand and T. R. Troutt, "A note on spanwise structure in the two-dimensional mixing layer," J. Fluid Mech. **97**, 771-781 (1980).

[50] P. Comte, M. Lesieur, and E. Lamballais, "Small-scale stirring of vorticity and a passive scalar in a 3D temporal mixing layer," Phys. Fluids A **4**, 2761-2778 (1992).

[51] P. Comte, J. H. Sivestrini, and P. Begou, "Streamwise vortices in large-eddy simulations of mixing layers," Eur. J. Mech., B: Fluids **17**, 615–637 (1998).

[52] C. D. Winant and F. K. Browand, "Vortex pairing: The mechanism of turbulent mixing-layer growth at moderate Reynolds number," J. Fluid Mech. **63**, 237–255 (1974).

[53] R. D. Moser and M. M. Rogers, "The three-dimensional evolution of a plane mixing layer: Pairing and transition to turbulence," J. Fluid Mech. **247**, 275–320 (1993).

[54] L. P. Bernal, "The statistics of the organized vortical structure in turbulent mixing layers," Phys. Fluids **31**, 2533–2543 (1988).

[55] A. D'Ovidio and C. M. Coats, "Coherent-structure evolution in turbulent mixing layers. Part 1: Experimental evidence," J. Fluid Mech. **737**, 466–498 (2013).

[56] J. Jimenez, "On the visual growth of a turbulent mixing layer," J. Fluid Mech. **96**, 447–460 (1980).

[57] D. W. Moore and P. G. Saffman, "The density of organised vortices in a turbulent mixing layer," J. Fluid Mech. **69**, 465–473 (1975).

[58] M. M. Rogers and R. D. Moser, "Direct simulation of a self-similar turbulent mixing layer," Phys. Fluids **6**, 903–923 (1994).

[59] G. L. Brown and A. Roshko, "Turbulent shear layers and wakes," J. Turbul. **13**, 1–32 (2012).